

LETTER • OPEN ACCESS

Observation of stabilized negative capacitance effect in hafnium-based ferroic films

To cite this article: Leilei Qiao *et al* 2024 *Mater. Futures* **3** 011001

View the [article online](#) for updates and enhancements.

You may also like

- [Negative capacitance in \(FeCoZr\)-\(PZT\) nanocomposite films](#)
T N Kotunowicz, J A Fedotova, P Zhukowski *et al.*
- [Comprehensive study of high pressure annealing on the ferroelectric properties of \$\text{Hf}_{0.5}\text{Zr}_{0.5}\text{O}_2\$ thin films](#)
Changyong Oh, Amit Tewari, Kyungkwan Kim *et al.*
- [A perspective on steep-subthreshold-slope negative-capacitance field-effect transistor](#)
Masaharu Kobayashi

Letter

Observation of stabilized negative capacitance effect in hafnium-based ferroic films

Leilei Qiao¹, Ruiting Zhao², Cheng Song^{1,*} , Yongjian Zhou¹, Qian Wang¹, Tian-Ling Ren² and Feng Pan^{1,*}

¹ Key Laboratory of Advanced Materials (MOE), School of Materials Science and Engineering, Tsinghua University, Beijing 100084, People's Republic of China

² Institute of Microelectronics & Beijing National Research Center for Information Science and Technology (BNRist), Tsinghua University, Beijing 100084, People's Republic of China

E-mail: songcheng@mail.tsinghua.edu.cn and panf@mail.tsinghua.edu.cn

Received 23 June 2023, revised 26 September 2023

Accepted for publication 19 October 2023

Published 3 January 2024



Abstract

A negative capacitance (NC) effect has been proposed as a critical pathway to overcome the 'Boltzmann tyranny' of electrons, achieve the steep slope operation of transistors and reduce the power dissipation of current semiconductor devices. In particular, the ferroic property in hafnium-based films with fluorite structure provides an opportunity for the application of the NC effect in electronic devices. However, to date, only a transient NC effect has been confirmed in hafnium-based ferroic materials, which is usually accompanied by hysteresis and is detrimental to low-power transistor operations. The stabilized NC effect enables hysteresis-free and low-power transistors but is difficult to observe and demonstrate in hafnium-based films. This difficulty is closely related to the polycrystalline and multi-phase structure of hafnium-based films fabricated by atomic layer deposition or chemical solution deposition. Here, we prepare epitaxial ferroelectric $\text{Hf}_{0.5}\text{Zr}_{0.5}\text{O}_2$ and antiferroelectric ZrO_2 films with single-phase structure and observe the capacitance enhancement effect of $\text{Hf}_{0.5}\text{Zr}_{0.5}\text{O}_2/\text{Al}_2\text{O}_3$ and $\text{ZrO}_2/\text{Al}_2\text{O}_3$ capacitors compared to that of the isolated Al_2O_3 capacitor, verifying the stabilized NC effect. The capacitance of $\text{Hf}_{0.5}\text{Zr}_{0.5}\text{O}_2$ and ZrO_2 is evaluated as -17.41 and -27.64 pF, respectively. The observation of the stabilized NC effect in hafnium-based films sheds light on NC studies and paves the way for low-power transistors.

Supplementary material for this article is available [online](#)

Keywords: negative capacitance effect, fluorite structure, hafnium-based ferroelectrics, antiferroelectric

* Authors to whom any correspondence should be addressed.



Original content from this work may be used under the terms of the [Creative Commons Attribution 4.0 licence](#). Any further distribution of this work must maintain attribution to the author(s) and the title of the work, journal citation and DOI.

1. Introduction

Due to the scaling of transistors, the inevitable short channel effect and drain-induced barrier lowering result in the performance degradation of subthreshold swing (SS) and the increase in static power dissipation, which have become key restrictions on the microelectronic industry [1]. A negative capacitance (NC) effect is proposed to realize SS smaller than 60 mV dec^{-1} and magnify the control effect of the gate over the channel by integrating the ferroelectric or antiferroelectric film into the gate oxide layer [2–4]. In particular, ferroelectricity and antiferroelectricity in hafnium-based oxides (e.g. $\text{Hf}_{0.5}\text{Zr}_{0.5}\text{O}_2$, ZrO_2) give rise to its emergence as an excellent material system and exploits a potential channel for the application of NC effect, due to their complementary-metal-oxide–semiconductor (CMOS) compatibility [5], ferroic property in ultrathin films [6, 7], high binding energy between metal cations and oxygen ions [8] and high permittivity compared to SiO_2 [9].

The NC effect can be categorized as a transient and stabilized one [10]. The former originates from the polarization switching and is accompanied by hysteresis [11–14], while the latter shows no hysteresis and theoretically stems either from a homogeneous vanishing of the polarization or from a complex multi-domain state both caused by the depolarization field [2, 10]. To date, the transient NC effect has been clearly confirmed in the hafnium-based materials by monitoring the charge and voltage trends [10, 15]. It was first reported in Ga-doped HfO_2 film by connecting the ferroelectric capacitor in series with an external resistor, and the charge exhibits an opposite variation trend with voltage during the polarization switching [12]. In transistors, the transient NC effect can lead to voltage amplification and SS reduction, meaning a negative capacitance field-effect transistor. Unfortunately, the transfer curves exhibit hysteretic characteristics, which are seriously adverse for low-power logic operations [16, 17], or are limited by the applied voltage [18–20]. From all these measurements, no capacitance enhancement of ferroic/dielectric in metal–insulator–metal (MIM) capacitors other than in isolated dielectric capacitors has been observed, which is considered to be solid evidence for a stabilized NC effect [10]. Although there has been much progress with respect to research into the transient NC effect, its transient and hysteretic nature limits its applications in low-power logic operations.

In contrast, the stabilized NC effect can produce a hysteresis-free and steep slope transfer curve, enabling the low-power operation of transistors. Although a stabilized NC effect has been observed in metal–oxide–semiconductor capacitors [21] or in MIM capacitors via calculating the polarization response versus voltage by applying a series of pulse voltages [22] or in transistors by measuring the SS, the observation of the stabilized NC effect in MIM capacitors via capacitance enhancement is absent. The hafnium-based films represented by ferroelectric $\text{Hf}_{0.5}\text{Zr}_{0.5}\text{O}_2$ (HZO) and antiferroelectric ZrO_2 , have polycrystalline and multi-phase structure when fabricated via atomic layer deposition (ALD) or chemical solution deposition (CSD) [7, 23–27].

The independent crystal orientation of each grain produces multidomain structure with random polar axes in hafnium-based films. The domain wall of ferroelectrics plays an important role in the NC effect [28]. However, the switching of domains inevitably induces hysteresis in transistors. In addition, the existence of non-polar phases, such as the monoclinic phase, which are in parallel with the negative capacitor, would also weaken the NC effect [29]. Although the hysteresis in some multi-phase and polycrystalline HZO films can be reduced to be very small [27, 30, 31], the counterclockwise hysteresis induced by the polarization switching [32, 33] is inevitable and never disappears. Moreover, the drain current range of SS smaller than 60 mV dec^{-1} is seriously limited. Here, by fabricating ferroelectric HZO and antiferroelectric ZrO_2 films with single phase, the stabilized NC effect has been successfully observed in both films from the small-signal capacitance enhancement. The demonstration of the stabilized NC effect in hafnium-based materials could pave the way to deeper understanding of the NC effect, and greatly promote the application of the NC effect in low-power devices.

2. Method

Materials Fabrication. The HZO and ZrO_2 films were grown on $\text{La}_{2/3}\text{Sr}_{1/3}\text{MnO}_3$ (LSMO) bottom electrodes by pulsed laser deposition (PLD) with a 248 nm wavelength KrF excimer laser from the corresponding targets. The LSMO films were deposited at 670°C under oxygen pressure of 100 mtorr. The HZO films were deposited at 750°C under oxygen background pressure of 23 mtorr. The ZrO_2 film was prepared at 770°C under oxygen pressure of 10 mtorr. After growth, the samples were annealed with 300 torr oxygen pressure under the deposition temperature for 30 min. The samples are then naturally cooled down to room temperature under the 300 torr oxygen pressure without any heating source. The thicknesses of HZO and ZrO_2 are 34 and 17.8 nm, respectively. The Al_2O_3 dielectric layer was deposited at 300°C by ALD. For electrical measurements, the Pt top electrodes were fabricated in a circular pattern with a diameter of $50 \mu\text{m}$ by standard photolithography and lift-off technologies.

Materials Characterization. The crystal structure of the ferroic materials was characterized by x-ray diffraction (XRD) using a Bruker diffractometer (D8 Discover, $\text{Cu K}\alpha$ radiation).

Electrical Properties. The ferroic properties were characterized by the capacitance and voltage response (C – V) using an Agilent B1520 multi-frequency capacitance measurement unit. During the measurements, a direct current (DC) voltage superposed by a 100 mV alternate current (AC) voltage was applied to the top electrode Pt, and the LSMO bottom electrode was grounded. The transient NC effect was measured by monitoring the charge and voltage variation trends under the voltage pulse. A voltage pulse is applied on a series circuit of ferroelectric capacitors and an external resistor of $3 \text{ k}\Omega$ using Agilent B1530. The pulse width, amplitude and rise time can be set on demand. Piezoelectric force microscope

(PFM) measurements were performed using a commercial atomic force microscope system (Cypher, Asylum Research). The bias is applied through the conductive tip and the bottom electrode was grounded. The amplitude and phase response to voltage were performed to characterize the ferroelectric and domain properties. During the measurements, the probe is in contact mode, and the bending of the cantilever reflects the vibration of the sample surface when applying voltage.

3. Results

3.1. Origin of the ferroelectric NC effect

The NC effect of ferroic materials is reported to originate from the negative curvature of the Landau energy landscape for the homogeneous structure of figure 1(a) [2, 34, 35]. Around $P = 0$ marked by the dotted line in figure 1(b), the capacitance C , which is proportional to the curvature ($C \propto (\frac{d^2G}{dP^2})^{-1}$) [32], is negative. The double-well energy landscape leads to a hysteresis-free S-shaped polarization response to the electric field, as displayed in figure 1(c), which is the ideal circumstance for the NC effect. Nevertheless, the HZO films fabricated by ALD [9, 36, 37] or CSD [25–27] are usually polycrystalline and multi-phase structure, and the energy state and circuit component are altered, as displayed in figures 1(d)–(f). Non-polar phases, such as monoclinic and tetragonal, coexist with the ferroelectric orthorhombic phase. When considering the influence of the non-polar part, the system can be taken to be a parallel structure of the polycrystalline ferroelectrics and non-polar dielectric phases, as shown in figure 1(e). The total capacitance C can be evaluated as $C = C_{FE} + C_{DE}$ according to the parallel principle of capacitors. Even though the ferroelectric capacitance C_{FE} presents as a negative value, the dielectric part unquestionably weakens the NC effect even making the NC effect disappear [26]. The polycrystalline structure with versatile crystalline orientations determines the multidomain structure of HZO films. The hysteresis usually occurs due to the nucleation and growth of reversed domains, which would produce a strong stray field at the interface between the ferroelectric and dielectric layers, as shown by the red dotted line in figure 1(f) [38–40]. The NC effect only occurs during the polarization switching, and disappears once the polarization switching is finished. This time-dependent NC effect is called the transient NC effect, which is not applicable to the logical operation of transistors and entails large power consumption [16, 17]. The multidomain-polycrystalline-multiphase structure in HZO films makes the NC effect weak and transient, which prevents the application of HZO films in future integrated circuits.

3.2. Ferroelectricity and transient NC effect of HZO film

In order to achieve a stabilized NC effect, we have deposited the HZO films by PLD, which is beneficial to the single-phase and single-domain structure in certain regions via the crystal lattice parameter matching of the SrTiO₃ (STO) substrate

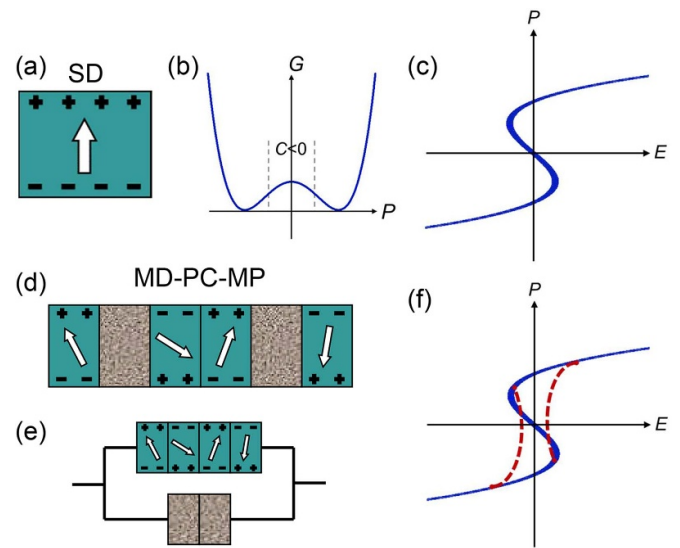


Figure 1. Ferroelectric NC effect in different structures.

(a) Single-domain (SD) structure for ferroelectrics. (b) Energy landscape effect of SD ferroelectrics. Regions around $P = 0$ marks the NC regions. (c) Polarization and electric field response (P - E) of SD ferroelectrics. (d) Multidomain, polycrystalline and multi-phase (MD-PC-MP) structure of ferroelectrics. (e) Parallel circuit of polar phase and non-polar phases. (f) P - E loop of multidomain ferroelectrics.

and LSMO bottom electrode. The thickness of the HZO film is 34 nm (figure S1, supporting information). Figure 2(a) shows the XRD spectrum of the STO/LSMO/HZO heterostructure. The peaks around 30° and 62° marked by purple rhombuses represent the (111) and (222) planes of HZO films with orthorhombic Pca2₁ crystal structure [41–43], suggesting the existence of ferroelectric properties. Diffraction peaks originating from other phases (such as monoclinic and tetragonal) or other orientations (such as (110) and (001)) are observed. Furthermore, the grazing incidence XRD of HZO (figure S2, supporting information) does not show any diffraction peaks, suggesting the single-phase structure. The single phase and strong texture along the [111] orientation of the HZO film contribute to the total capacitance of the HZO films and create an essential prerequisite for the realization of the stabilized NC effect, as discussed above. The ferroelectric property is measured via small signal capacitance, ferroelectric loop and PFM methods. A small signal capacitance response towards voltage (C - V) is performed by superimposing a 100 mV AC voltage on the DC voltage at a 100 kHz frequency. As shown in figure 2(b), the C - V loop displays a butterfly shape, and two peaks under negative and positive electric fields are caused by the polarization switching, which is a classic characteristic of ferroelectrics [21, 44]. The inset of figure 2(b) shows the unit cell of HZO. The Hf and Zr atoms distribute at the vertex and face center positions of the unit cell, and the oxygen atoms distribute at the center position of eight small cubics. In fluorite ferroelectrics, the oxygen displacement is described as the root of the spontaneous polarization and polarization switching [45]. The hysteresis loop measured

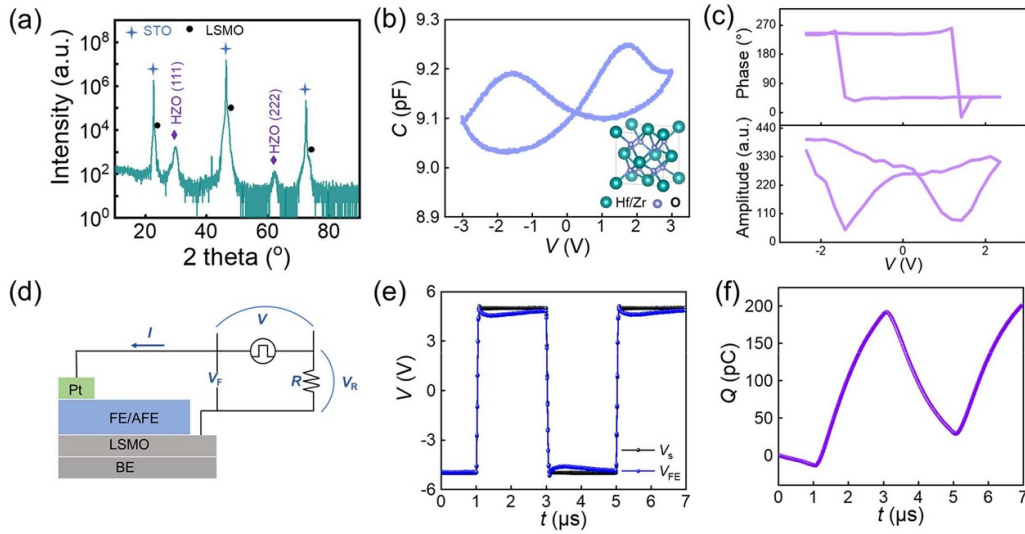


Figure 2. Ferroelectricity and transient NC effect of the 34 nm HZO film. (a) XRD results of the STO/LSMO/HZO structure. HZO film shows strong texture with (111) out-of-plane orientation in orthorhombic crystal structure, which is marked by a purple rhombus. Blue stars and black dots mark the diffraction peaks of the STO substrate and LSMO bottom electrode, respectively. (b) Capacitance and voltage response (C - V) of the HZO capacitor with a butterfly shape, displaying a classic ferroelectric property. Inset shows the schematic of the unit cell of HZO. (c) Local PFM hysteresis phase loop (top panel) and amplitude loop (bottom panel). (d) Schematic setup of transient NC effect observation for STO/LSMO/HZO/Pt capacitor in series with an external resistor. (e) Source voltage and the response of voltage across the ferroelectric layer as a function of time t . (f) Charge response of the ferroelectric capacitor.

by the ferroelectric analyzer shows ferroelectric characteristics with about $20 \mu\text{C cm}^{-2}$ saturation polarization (figure S3, supporting information). The low leakage current of HZO films can support accurate measurements of P - V and C - V response (figure S4, supporting information). We have also performed PFM spectroscopy measurements to embody the local ferroelectricity, as shown in figure 2(c) [29]. The phase loop displays 180° domain switching, and the amplitude loop exhibits a good butterfly shape. The phase PFM image shows 180° contrast of the central region of $1.5 \times 1.5 \mu\text{m}^2$ poled by a positive bias after the force of a negative bias from the poled region by negative bias in the $3 \times 3 \mu\text{m}^2$ area is shown, indicating the 180° polarization switching. The amplitude of the PFM image shows a clear domain wall on the boundary separating the opposite poled regions (figure S5, supporting information). Along with the P - V and C - V responses, robust ferroelectricity is demonstrated in HZO films.

The PFM phase image in the $30 \mu\text{m} \times 30 \mu\text{m}$ area shows almost exactly the same polar orientation, indicating its single-domain structure in this area of the HZO film (figure S6(a), supporting information). The domains can be switched by the electric field. By applying $+6 \text{ V}$ and -6 V voltage in the central region ($3.5 \mu\text{m} \times 3.5 \mu\text{m}$) of figure S5(a), clear domain switching is observed (figure S6(b), supporting information). The -6 V voltage in the central regions drives the domain to switch the polarization vectors to the opposite direction. We have also performed the amplitude and phase response at the random position of figure S5(a). A butterfly-shape amplitude response and almost 180° phase switching are observed (figures S6(c) and 6(d), supporting information), which further verify the ferroelectricity of the HZO film.

The ferroelectric LSMO/HZO/Pt capacitor shows a clear transient NC effect. Figure 2(d) shows the schematic setup. The ferroelectric capacitor is connected in series with an external resistor of $3 \text{ k}\Omega$. The voltage across the ferroelectric capacitor V_F , current I and charge Q are monitored, as shown in figures 2(e) and (f). When applying a voltage V_s from -5 to 5 V , voltage V_F abruptly increases to about 5 V , then decreases slowly for $0.2 \mu\text{s}$. In the meantime, charge Q keeps increasing, and then increases continuously until V_s decreases to zero. It worth noting that voltage V_F also has an opposite variation trend with the charge Q when once a source voltage from 5 to -5 V is applied. The opposite trends suggest the transient NC effect according to $C = \frac{dQ}{dV}$. The transient NC effect is caused by the polarization switching of ferroelectric HZO films. Thus, it occurs when voltage V_s switches directions and disappears once the stable polarization state is achieved. The corresponding polarization responses with voltage also display negative differential capacitance under different series resistors (figure S7, supporting information). When no resistor is connected, the transient NC effect disappears, indicating the important role of the resistor in slowing down the charge compensation (figure S8, supporting information). The time-dependent transient NC effect gives rise to hysteretic characteristics and is detrimental to the low-power operation of transistors.

3.3. Stabilized NC effect of ferroelectric HZO film

When two capacitors are connected in series, the total capacitance is smaller than that of any separate capacitor according to the capacitance series principle $\frac{1}{C} = \frac{1}{C_1} + \frac{1}{C_2}$ due to the limitation of thermodynamic stability, where C refers to the

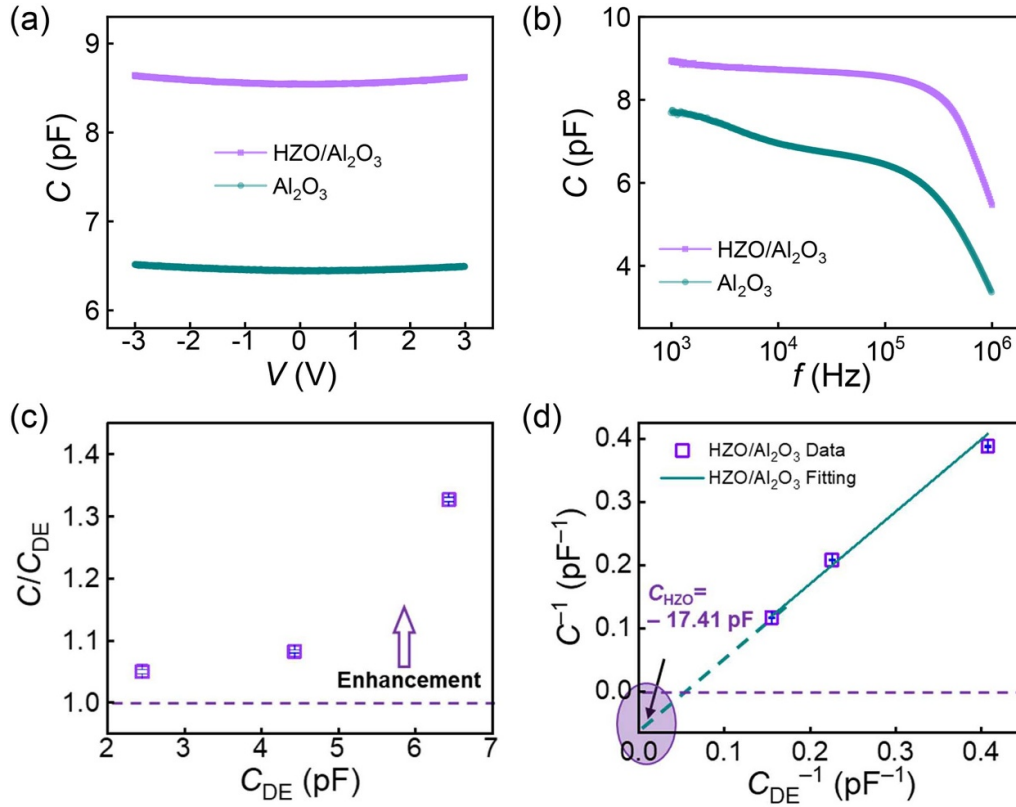


Figure 3. Stabilized NC effect of ferroelectric HZO films. Capacitance comparison of HZO/Al₂O₃ capacitor and isolated Al₂O₃ capacitor with (a) voltage from -3 to 3 V, (b) frequency from 1 kHz– 1 MHz. (c) Capacitance enhancement factor C/C_{DE} in HZO/Al₂O₃ capacitor with different dielectric layer thicknesses as a function of the dielectric capacitance C_{DE} . For each capacitor, three devices are measured, and the corresponding error bar is shown by blue marks. (d) Inverse series capacitance C^{-1} as a function of the inverse dielectric capacitance C_{DE}^{-1} . Intercept represents the inverse of the ferroelectric HZO layer, indicating the HZO layer has negative differential capacitance.

total capacitance, and C_1 , C_2 (C_1 , $C_2 > 0$) denote respective component capacitance of the series structure. This principle is also true when one of the capacitors C_1 displays negative differential capacitance as long as the total capacitance C remains positive. In this situation, the total capacitance C is larger than C_2 . From this point, the NC effect can be verified by the capacitance enhancement in a series system. It is also considered as solid evidence to verify the stabilized NC effect because capacitance enhancement is not possible for the transient NC effect [10].

Via the method we referred to above, we have fabricated the Al₂O₃ (10 nm) and HZO/Al₂O₃ (10 nm) capacitors where Al₂O₃ is normal dielectric and HZO is ferroelectric with strong texture and single orthorhombic phase. The Al₂O₃ layer is added to stabilize the NC region and prevent the screening of bound polarization charge by free electrons on the metal electrodes. As shown in figure 3(a), the capacitance of the HZO/Al₂O₃ heterostructure is approximately 8.6 pF, which is measured at 100 kHz frequency and 100 mV AC voltage superimposed on the DC voltage. This value is evidently larger than that of the isolated Al₂O₃ capacitors (6.5 pF). Both capacitors have the same device area and the Al₂O₃ layer is deposited simultaneously in the same chamber that has the same thickness and properties. In addition,

considering that the Al₂O₃ layer is a normal dielectric whose capacitance can be considered to be a constant, the capacitance enhancement of the ferroelectric/dielectric heterostructure capacitor is indeed caused by the ferroelectric HZO layer. Polarization coupling is considered to be a possible reason for the capacitance enhancement of the ferroelectric/dielectric capacitor, but it cannot be the origin of our device structure because the dielectric layer we have adopted is amorphous Al₂O₃ where polarization is hard to generate due to its amorphous character. Moreover, in order to exclude the influence of the Maxwell–Wagner effect [46], which could also induce the increase in capacitance, we have performed capacitance measurements with the frequency from 1 kHz–1 MHz, as shown in figure 3(b). The capacitance of the HZO/Al₂O₃ capacitor decreases with frequency monotonously but is always larger than that of any isolated Al₂O₃ capacitor under all the frequency ranges (figure S9, supporting information). This effect is closely related to the interface numbers, so the Maxwell–Wagner effect has negligible influence on the capacitance enhancement given that there is a single interface in our device structure. The results clearly show capacitance enhancement compared to the Al₂O₃ capacitor under all frequency ranges. This demonstrates that the ferroelectric HZO film has a stabilized NC effect.

To further verify the capacitance enhancement effect due to the stabilized NC effect, we have connected the HZO film with Al_2O_3 layers of different thicknesses (10, 20, 30 nm). The Al_2O_3 films of 10, 20 and 30 nm thicknesses have a low leakage current lower than 10^{-11} A and a low leakage current can be maintained through a large voltage range (figure S10, supporting information). Then, we plotted the capacitance enhancement factor C/C_{DE} (defined as the ratio of capacitance of HZO/ Al_2O_3 capacitor C and the isolated dielectric Al_2O_3 capacitor C_{DE} , C/C_{DE}) as a function of dielectric capacitance C_{DE} , as shown in figure 3(c). All the HZO/ Al_2O_3 capacitors with different Al_2O_3 thicknesses show capacitance enhancement ($C/C_{\text{DE}} > 1$), demonstrating the stabilized NC effect under proper capacitance matching conditions. The small difference between the devices, as shown by the error bars, indicates the good uniformity and the accuracy of the measurements. When two capacitors are connected in series, the series principle ($\frac{1}{C} = \frac{1}{C_{\text{F}}} + \frac{1}{C_{\text{DE}}}$) decides that the inverse of the total capacitance has a linear dependence on the inverse of the capacitance of the dielectric layer, and the intercept represents the inverse of the ferroelectric capacitance. We have summarized the capacitance data in figure 3(d). The inverse capacitance of the HZO/ Al_2O_3 capacitor C^{-1} has a good linear dependence as a function of the inverse capacitance of the Al_2O_3 capacitor C_{DE}^{-1} . After fitting, the slope is about 1, and the degree of fitting (R^2) is 0.98965, which coincides well with the series principle. The capacitance of the HZO is evaluated by the intercept as -17.41 pF. The capacitance enhancement occurs in different devices with the same structure and thickness and in devices with different Al_2O_3 layer thicknesses, which strongly indicates the existence of capacitance enhancement, and demonstrates the stabilized NC effect in ferroelectric HZO films. The NC (also permittivity) has great potential in the future microelectronics industry [47–50].

3.4. Stabilized NC effect of antiferroelectric ZrO_2 film

ZrO_2 , which has a similar fluorite structure to HZO, is also a potential CMOS-compatible material for low-power memories with high-speed operation and good endurance performance [50, 51]. The difference is that ZrO_2 displays a non-polar state in the absence of an electric field, instead of an anti-polar state, then undergoes a phase transition from tetragonal $\text{P4}_2/\text{nmc}$ phase (central-symmetric) to orthorhombic $\text{Pca}2_1$ structure (non-central-symmetric) with polar state under a large electric field [52–54]. We have performed similar stabilized NC effect measurements on antiferroelectric ZrO_2 films with the same setup as mentioned above for HZO. The ZrO_2 film has a tetragonal crystal structure with (110) out-of-plane orientation, as marked by a peak around 35° , which gives the possibility of antiferroelectric characteristics (figure S11(a), supporting information) [55]. The ZrO_2 films have a low leakage current lower than 10^{-10} A, which guarantees the reliability of electrical measurements (figure S4(b), supporting information). The C - V loop of the LSMO/ ZrO_2 /Pt capacitor

displays a double-butterfly shape, indicating its antiferroelectric properties (figure S11(b), supporting information).

In order to explore the capacitance enhancement effect, we connected ZrO_2 film with 10 nm (figure S1, supporting information) in series with a normal dielectric Al_2O_3 film (10 nm) to compare the capacitance and verify the NC effect. As exhibited in figure 4(a), the antiferroelectric heterostructure $\text{ZrO}_2/\text{Al}_2\text{O}_3$ capacitor has a capacitance of about 7.8 pF, which is larger than that of the Al_2O_3 capacitor with the same thickness. As shown by the frequency-dependent capacitance measurement in figure 4(b), the capacitance of the antiferroelectric heterostructure capacitor is always larger than that of the Al_2O_3 capacitor under the frequency from 1 kHz–1 MHz. The capacitance enhancement through voltages and frequencies clearly demonstrates the static NC effect in antiferroelectric ZrO_2 films. Not limited by a specific capacitance, the capacitance enhancement is observed in the $\text{ZrO}_2/\text{Al}_2\text{O}_3$ capacitor with the different dielectric layer thicknesses (10, 20, 30 nm), as shown in figure 4(c). The inverse capacitance of the $\text{ZrO}_2/\text{Al}_2\text{O}_3$ capacitor C^{-1} has a good linear dependence as a function of the inverse capacitance of the Al_2O_3 capacitor C_{DE}^{-1} . The slope of the linear fitting is about 1, and the fitting degree is 0.99953. The capacitance of the antiferroelectric layer ZrO_2 is evaluated by the intercept of the linear fitting as -27.64 pF from figure 4(d). The stabilized NC effect is clearly verified in the antiferroelectric ZrO_2 films. We have also observed the transient NC effect in the LSMO/ ZrO_2 /Pt capacitors with different resistors in series. When no resistor is connected, the antiferroelectric capacitor does not show a transient NC effect (figure S12, supporting information). The transient NC effect becomes more obvious with the resistance increasing (figure S13, supporting information).

ZrO_2 is in the non-polar tetragonal $\text{P4}_2/\text{nmc}$ phase when no electric field is applied and undergoes a first-order structural phase transition into the polar orthorhombic $\text{Pca}2_1$ phase by application of an electric field over its coercive field. The polar orthorhombic $\text{Pca}2_1$ phase has been shown to be responsible for the ferroelectric behavior. The negative curvature of the Landau energy curve enables the antiferroelectric film potential to be affected by NC. The NC effect can be observed during the phase transition from non-polar to polar phases. When the antiferroelectric film is connected to a dielectric film with proper capacitance matching, the energy state is altered, and the forbidden thermodynamic region is stabilized. Although the whole system holds a positive capacitance, the antiferroelectric film exhibits negative differential capacitance.

The ALD and CSD fabricated films have polycrystalline structures with versatile polar orientations. Multidomain structures are inevitably formed in different grains due to their independent polar axes. The nucleation of the reversed domain induces a strong stray field at the interface of the HZO/ Al_2O_3 stack, and the resultant transient NC effect. Even though NC effect still occurs when reverse domain nucleation and growth are not involved, it needs a large domain wall mobility and an ultrahigh viscosity coefficient [19, 20, 29]. That is why hysteresis-free transfer curves can only be obtained under high-voltage sweep rate, and the hysteresis appears

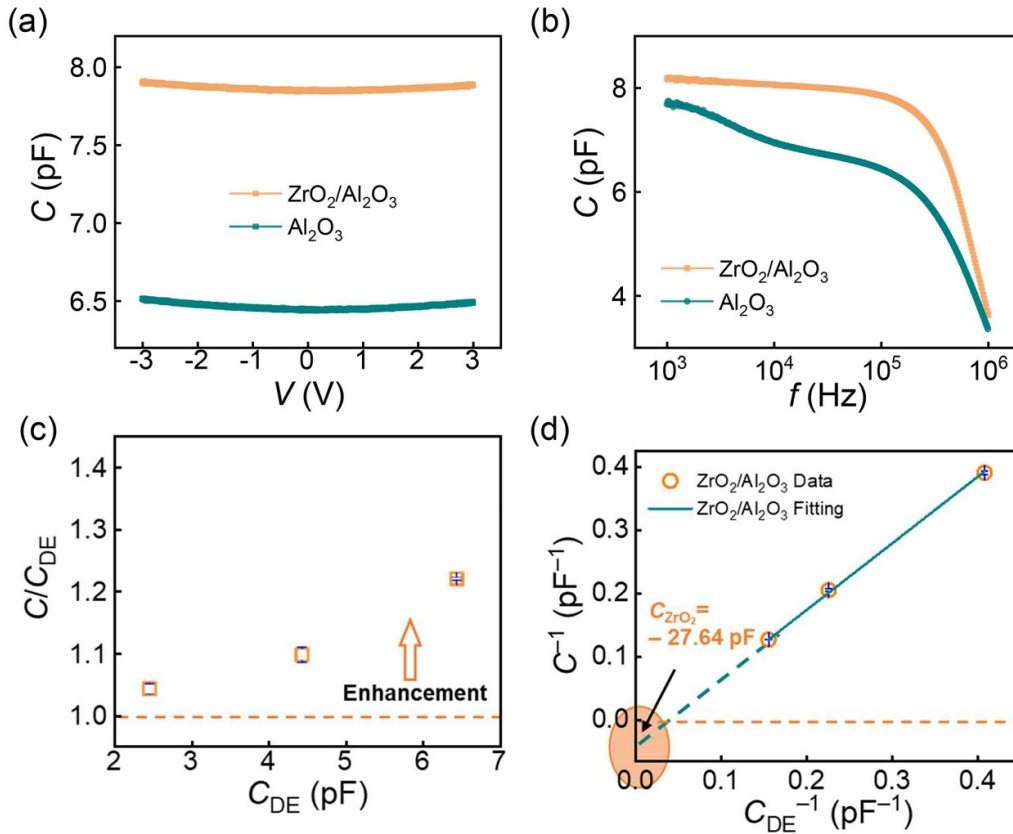


Figure 4. Stabilized NC effect of antiferroelectric ZrO₂ film. Capacitance comparison of the ZrO₂/Al₂O₃ capacitor and isolated Al₂O₃ capacitor as a function of (a) voltage and (b) frequency. (c) Capacitance enhancement factor C/C_{DE} in the ZrO₂/Al₂O₃ capacitor with different dielectric layer thicknesses as a function of the dielectric capacitance C_{DE} . For each capacitor, three devices are measured, and the corresponding error bar is shown by blue marks. (d) Inverse series capacitance C^{-1} as a function of the inverse dielectric capacitance C_{DE}^{-1} . Intercept represents the inverse of the antiferroelectric ZrO₂ layer, indicating that the ZrO₂ layer has negative differential capacitance of -27.64 pF.

when decreasing the sweep rate [17]. Hysteresis-free operation and low threshold voltage are strongly pursued [30]. The NC effect achieved by improving the sweep rate is an extrinsic method, which we are reluctant to use for low-power operations because of the limited SS reduction. Moreover, monoclinic, tetragonal and orthorhombic phases usually coexist in the films fabricated by ALD and CSD due to the limitation of free energy and activation barriers [9]. This portion of positive capacitance from the non-polar phases is parallel to the ferroelectric capacitor, and it would seriously weaken the effect of capacitance enhancement [29]. A hysteresis-free NC effect is obtained in HZO/Ta₂O₅ heterostructure capacitors via pulse electrical measurements, generating the first experimental observation of ‘S’-shape P - E curve [18]. Nevertheless, this NC effect only occurs when the applied voltage is larger than 5 V, which is detrimental to low-power applications [19, 20]. Here, by adopting hafnium-based films fabricated by PLD, which have a single-phase structure with certain domain orientation in small regions, the influence of the above factors is effectively avoided. Thus, the stabilized NC effect is observed via capacitance enhancement in epitaxial HZO and ZrO₂ films. The stabilized NC effect in films expands the application of oxides [56–59] and is expected to reduce the power consumption of transistors.

4. Conclusion

In summary, we have observed the stabilized NC effect in ferroelectric HZO and antiferroelectric ZrO₂ films via small signal capacitance enhancement measurements. The capacitance of HZO and ZrO₂ films is evaluated to be -17.41 and -27.64 pF, respectively. The stabilized NC effect can effectively resolve the power dissipation due to the hysteresis, which is common for the transient NC effect. The demonstration of a stabilized NC effect unveils the mist of its existence, deepens our understanding of the NC effect and promotes the application of the NC effect in low-power devices.

5. Future perspectives

Recently, the emergence of hafnium-based materials [5–7] and 2D ferroelectrics [60] has paved new ways for the scaling of integration circuits. The hafnium-based materials with fluorite structure, which is CMOS compatible, have become more and more popular for their fabrication method, permittivity and sub-nanometer ferroic properties in the application of memory or logic transistors [61, 62]. The observation of stabilized NC effect in hafnium-based films has laid the foundation for its

application in future integrated circuits. The implementation of NC effect in capacitors would favor the improvement of energy storage density and efficiency of supercapacitors and inspire research into the NC effect in transistors. The implementation of NC effect in transistors would greatly reduce SS to overcome the Boltzmann tyranny, thus promoting the development of low-power devices.

Acknowledgments

The authors gratefully acknowledge the support of the National Key R&D Program of China (Grant No. 2021YFB3601301), the National Natural Science Foundation of China (Grant Nos. 52225106 and 12241404) and the Natural Science Foundation of Beijing, China (Grant No. JQ20010).

Conflict of interest

The author declare no conflicts of interests.

Authors' contributions

F Pan, C Song and L Qiao conceived and supervised the project. L Qiao and R Zhao deposited the films and fabricated the devices. L Qiao and Y Zhou L Qiao and Y Zhou performed the electrical measurements. F Pan, C Song, L Qiao, R Zhao, Y Zhou and Q Wang performed the data analysis and co-wrote the manuscript. All the authors discussed the results and revised the manuscript.

Funding sources

The National Key R&D Program of China (Grant No. 2021YFB3601301), the National Natural Science Foundation of China (Grant No. 52225106 and 12241404) and the Natural Science Foundation of Beijing, China (Grant No. JQ20010).

ORCID iD

Cheng Song  <https://orcid.org/0000-0002-7651-9031>

References

- [1] Theis T N and Solomon P M 2010 It's time to reinvent the transistor! *Science* **327** 1600
- [2] Salahuddin S and Datta S 2008 Use of negative capacitance to provide voltage amplification for low power nanoscale devices *Nano Lett.* **8** 405–10
- [3] Salvatore G A, Bouvet D and Ionescu A M 2008 Demonstration of subthreshold swing smaller than 60 mV/decade in Fe-FET with P(VDF-TrFE)/SiO₂ gate stack *IEEE Int. Electron Devices Meeting (IEDM)* pp 167–70
- [4] Qiao L, Song C, Sun Y, Fayaz M U, Lu T, Yin S, Chen C, Xu H, Ren T-L and Pan F 2021 Observation of negative capacitance in antiferroelectric PbZrO₃ films *Nat. Commun.* **12** 4215
- [5] Müller J *et al* 2013 Ferroelectric hafnium oxide: a CMOS-compatible and highly scalable approach to future ferroelectric memories *IEEE Int. Electron Devices Meeting* pp 10.8.1–4
- [6] Lee H-J, Lee M, Lee K, Jo J, Yang H, Kim Y, Chae S C, Waghmare U and Lee J H 2020 Scale-free ferroelectricity induced by flat phonon bands in HfO₂ *Science* **369** 6509
- [7] Cheema S S *et al* 2020 Enhanced ferroelectricity in ultrathin films grown directly on silicon *Nature* **580** 478–82
- [8] Park M H, Kim H J, Kim Y J, Lee W, Kim H K and Hwang S C 2013 Effect of forming gas annealing on the ferroelectric properties of Hf_{0.5}Zr_{0.5}O₂ thin films with and without Pt electrodes *Appl. Phys. Lett.* **102** 112914
- [9] Schroeder U, Park M H, Mikolajick T and Hwang C S 2022 The fundamentals and applications of ferroelectric HfO₂ *Nat. Rev. Mater.* **7** 653–69
- [10] Hoffmann M, Slesazek S, Mikolajick T and Hwang C S 2019 *Ferroelectricity in Doped Hafnium Oxide Duxford* (Woodhead Publishing) p 473
- [11] Khan A I, Chatterjee K, Brian W, Drapcho S, You L, Serrao C, Bakaul S R, Ramesh R and Salahuddin S 2015 Negative capacitance in a ferroelectric capacitor *Nat. Mater.* **14** 5
- [12] Hoffmann M, Pešić M, Chatterjee K, Khan A I, Salahuddin S, Slesazek S, Schroeder U and Mikolajick T 2016 Direct observation of negative capacitance in polycrystalline ferroelectric HfO₂ *Adv. Funct. Mater.* **26** 8643–9
- [13] Saha A K, Datta S and Gupta S K 2018 “Negative capacitance” in resistor-ferroelectric and ferroelectric-dielectric networks: apparent or intrinsic? *J. Appl. Phys.* **123** 105102
- [14] Hoffmann M, Khan A I, Serrao C, Lu Z, Salahuddin S, Pešić M, Slesazek S, Schroeder U and Mikolajick T 2018 Ferroelectric negative capacitance domain dynamics *J. Appl. Phys.* **123** 184101
- [15] Chen J-D, Han W-H, Yang C, Zhao X-S, Guo Y-Y, Zhang X-D and Yang F-H 2020 Recent research progress of ferroelectric negative capacitance field effect transistors *Acta Phys. Sin.* **69** 137701
- [16] Hoffmann M, Slesazek S and Mikolajick T 2021 Progress and future prospects of negative capacitance electronics: a materials perspective *APL Mater.* **9** 020902
- [17] Wang Y *et al* 2020 Record-low subthreshold-swing negative-capacitance 2D field-effect transistors *Adv. Mater.* **32** 2005353
- [18] Hoffmann M, Fengler F P G, Herzig M, Mittmann T, Max B, Schroeder U, Negrea R, Lucian P, Slesazek S and Mikolajick T 2019 Unveiling the double-well energy landscape in a ferroelectric layer *Nature* **565** 464–7
- [19] Rollo T, Blanchini F, Giordano G, Specogna R and Esseni D 2019 Revised analysis of negative capacitance in ferroelectric-insulator capacitors: analytical and numerical results, physical insight, comparison to experiments *IEEE Annual Inter. Electron Devices Meeting* (<https://doi.org/10.1109/IEDM19573.2019.8993436>)
- [20] Esseni D and Fontanini R 2021 Macroscopic and microscopic picture of negative capacitance operation in ferroelectric capacitors *Nanoscale* **13** 9641–50
- [21] Cheema S S *et al* 2022 Ultrathin ferroic HfO₂–ZrO₂ superlattice gate stack for advanced transistors *Nature* **604** 65–71
- [22] Jo S *et al* 2023 Negative differential capacitance in ultrathin ferroelectric Hafnia *Nat. Electron.* **6** 390–7
- [23] Park M H, Kim H J, Kim Y J, Lee W, Moon T and Hwang C S 2013 Evolution of phases and ferroelectric properties of thin Hf_{0.5}Zr_{0.5}O₂ films according to the thickness and annealing temperature *Appl. Phys. Lett.* **102** 242905
- [24] Ohtaka O, Fukui H, Kunisada T and Fujisawa T O 2004 Phase relations and volume changes of hafnia under high pressure *J. Am. Ceram. Soc.* **84** 5

- [25] Starschich S, Griesche D, Schneller T, Waser R and Bottger U 2014 Chemical solution deposition of ferroelectric yttrium-doped hafnium oxide films on platinum electrode *Appl. Phys. Lett.* **104** 202903
- [26] Hsain H A, Lee Y, Materano M, Mittmann T, Payne A, Mikolajick T, Schroeder U, Parsons G N and Jones J L 2022 Many routes to ferroelectric HfO₂: a review of current deposition methods *J. Vac. Sci. Technol. A* **40** 010803
- [27] Pujar P, Cho H, Gandla S, Naqi M, Hong S and Kim S 2021 Sub-thermionic negative capacitance field effect transistors with solution combustion-derived Hf_{0.5}Zr_{0.5}O₂ *Adv. Funct. Mater.* **31** 2103748
- [28] Song J, Qi Y, Xiao Z, Wang K, Li D, Kim S-H, Kingon A I, Rappe A M and Hong X 2022 Domain wall enabled steep slope switching in MoS₂ transistors towards hysteresis-free operation *npj 2D Mater. Appl.* **6** 77
- [29] Park H W, Oh M and Hwang C S 2022 Negative capacitance from the inhomogenous stray field in a ferroelectric–dielectric structure *Adv. Funct. Mater.* **32** 2200389
- [30] Cho H W, Pujar P, Choi M, Kang S, Hong S, Park J, Baek S, Kim Y, Lee J and Kim S 2021 Direct growth of orthorhombic Hf_{0.5}Zr_{0.5}O₂ thin films for hysteresis-free MoS₂ negative capacitance field-effect transistors *npj 2D Mater. Appl.* **5** 1–8
- [31] Cho H, Pujar P, Choi M, Naqi M, Cho Y, Rho H Y, Lee J and Kim S 2021 Expediently crystallized pure orthorhombic-Hf_{0.5}Zr_{0.5}O₂ for negative capacitance field effect transistors *ACS Appl. Mater. Interfaces* **13** 60250–60
- [32] Khan A I, Keshavarzi A and Datta S 2020 The future of ferroelectric field-effect transistor technology *Nat. Electron.* **3** 588–97
- [33] Zhang Z, Su M, Li G, Wang J, Zhang X, Ho J C, Wang C, Wan D, Liu X and Liao L 2020 Stable hysteresis-free MoS₂ transistors with low-k/high-k bilayer gate dielectrics *IEEE Electron. Device Lett.* **41** 1036–9
- [34] Zubko P, Wojdeł J C, Hadjimichael M, Fernandez-Pena S, Sené A, Luk'yanchuk I, Triscone J-M and Íñiguez J 2016 Negative capacitance in multidomain ferroelectric superlattices *Nature* **534** 15
- [35] Yadav A K *et al* 2019 Spatially resolved steady-state negative capacitance *Nature* **565** 468–71
- [36] Park M H, Lee Y H and Hwang C S 2019 Understanding ferroelectric phase formation in doped HfO₂ thin films based on classical nucleation theory *Nanoscale* **11** 19477–87
- [37] Park M H, Lee Y H, Mikolajick T, Schroeder U and Hwang C S 2019 Thermodynamic and kinetic origins of ferroelectricity in fluorite structure oxides *Adv. Electron. Mater.* **5** 1800522
- [38] Zhao D, Lenz T, Gelinck G H, Groen P, Damjanovic D, de Leeuw D M and Katsouras I 2019 Depolarization of multidomain ferroelectric materials *Nat. Commun.* **10** 2547
- [39] Luk'yanchuk I, Tikhonov Y, Sené A, Razumnaya A and Vinokur V M 2019 Harnessing ferroelectric domains for negative capacitance *Commun. Phys.* **2** 22
- [40] Park H W, Roh J, Lee Y B and Hwang C S 2019 Modeling of negative capacitance in ferroelectric thin films *Adv. Mater.* **31** 1805266
- [41] Wei Y *et al* 2018 A rhombohedral ferroelectric phase in epitaxially strained Hf_{0.5}Zr_{0.5}O₂ thin films *Nat. Mater.* **17** 1095–100
- [42] Yoong H Y *et al* 2018 Epitaxial ferroelectric Hf_{0.5}Zr_{0.5}O₂ thin films and their implementations in memristors for brain-inspired computing *Adv. Funct. Mater.* **28** 1806037
- [43] Estandía S, Dix N, Gazquez J, Fina I, Lyu J, Chisholm M F, Fontcuberta J and Sánchez F 2019 Engineering ferroelectric Hf_{0.5}Zr_{0.5}O₂ thin films by epitaxial stress *ACS Appl. Electron. Mater.* **1** 1449–57
- [44] Pintilie L, Lisca M and Alexe M 2005 Polarization reversal and capacitance-voltage characteristic of epitaxial Pb(Zr,Ti)O₃ layers *Appl. Phys. Lett.* **86** 192902
- [45] Luo Q *et al* 2020 A highly CMOS compatible hafnia-based ferroelectric diode *Nat. Commun.* **11** 1391
- [46] Catalan G, O'Neill D, Bowman R M and Gregg J M 2000 Relaxor features in ferroelectric superlattices: a maxwell–wagner approach *Appl. Phys. Lett.* **77** 3078–80
- [47] Zhang Z *et al* 2022 Flexible polystyrene/graphene composites with epsilon-near-zero properties *Adv. Compos. Hybrid Mater.* **5** 1054–66
- [48] Xie P *et al* 2022 Recent advances in radio-frequency negative dielectric metamaterials by designing heterogeneous composites *Adv. Compos. Hybrid Mater.* **5** 679–95
- [49] Wu H, Zhong Y, Tang Y, Huang Y, Liu G, Sun W, Xie P, Pan D, Liu C and Guo Z 2022 Precise regulation of weekly negative permittivity in CaCu₃Ti₄O₁₂ metacomposites by synergistic effects of carbon nanotubes and grapheme *Adv. Compos. Hybrid Mater.* **5** 419–30
- [50] Chang S C *et al* 2021 FeRAM using anti-ferroelectric capacitors for high-speed and high-density embedded memory 2021 *IEEE Inter. Electron Devices Meeting (IEDM)* pp 33.2.1–4
- [51] Yan X *et al* 2019 Robust Ag/ZrO₂/WS₂/Pt memristor for neuromorphic computing *ACS Appl. Mater. Interfaces* **11** 48029–38
- [52] Hoffmann M *et al* 2022 Antiferroelectric negative capacitance from a structural phase transition in zirconia *Nat. Commun.* **13** 1228
- [53] Ali F, Ali T, Lehninger D, Sunbul A, Viegas A, Sachdeva R, Abbas A, Czernohorsky M and Seidel K 2022 Fluorite-structured ferroelectric and antiferroelectric materials: a gateway of miniaturized electronic devices *Adv. Funct. Mater.* **32** 2201737
- [54] Cheema S S *et al* 2022 Emergent ferroelectricity in subnanometer binary oxide films on silicon *Science* **5** 376
- [55] Luo X, Toprasertpong K, Takenaka M and Takagi S 2021 Antiferroelectric properties of ZrO₂ ultra-thin films prepared by atomic layer deposition *Appl. Phys. Lett.* **118** 232904
- [56] Gao S *et al* 2022 Highly transmitted silver nanowires-SWCNTs conductive flexible film by nested density structure and aluminum-doped zinc oxide capping layer for flexible amorphous silicon solar cells *J. Mater. Sci. Technol.* **126** 152–60
- [57] Hou C *et al* 2023 Boosted lithium storage performance by local build-in electric field derived by oxygen vacancies in 3D holey N-doped carbon structure decorated with molybdenum dioxide *J. Mater. Sci. Technol.* **142** 185–95
- [58] Ma R *et al* 2022 Enhanced energy storage of lead-free mixed oxide core double-shell barium strontium zirconate titanate@magnesium aluminate@zinc oxide-boron trioxide-silica ceramic nanocomposites *Adv. Compos. Hybrid Mater.* **5** 1477–89
- [59] Wu N, Zhao B, Chen X, Hou C, Huang M, Alhadhrami A, Mersal G A M, Ibrahim M M and Tian J 2022 Dielectric properties and electromagnetic simulation of molybdenum disulfide and ferric oxide-modified Ti₃C₂T_x MXene hetero-structure for potential microwave absorption *Adv. Compos. Hybrid Mater.* **5** 1548–56
- [60] Jiang X *et al* 2022 Manipulation of current rectification in van der Waals ferroionic CuInP₂S₆ *Nat. Commun.* **13** 574
- [61] Dai S *et al* 2022 Robustly stable ferroelectric polarization states enable long-term nonvolatile storage against radiation in hfo₂-based ferroelectric field-effect transistors *ACS Adv. Appl. Mater. Interfaces* **14** 51459–67
- [62] Liao J, Dai S, Peng R-C, Yang J, Zeng B, Liao M and Zhou Y 2023 HfO₂-based ferroelectric thin film and memory device applications in the post-Moore era: a review *Fundam. Res.* **3** 332–45